Articles

Distal Ligand Reactivity and Quaternary Structure Studies of Proximally Detached Hemoglobins†

Doug Barrick,*,‡ Nancy T. Ho,§ Virgil Simplaceanu,§ and Chien Ho§

T. C. Jenkins Department of Biophysics, Johns Hopkins University, 3400 North Charles Street, Baltimore Maryland 21218, and Department of Biological Sciences, Carnegie Mellon University, 4400 Fifth Avenue, Pittsburgh, Pennsylvania 15213-2683

Received September 14, 2000; Revised Manuscript Received January 9, 2001

ABSTRACT: The linkage between the proximal histidines and the proximal polypeptide in normal adult human hemoglobin (Hb A) has been proposed to play a major role in transmitting allosteric effects between oxygen binding sites [Perutz, M. F. (1970) *Nature 228*, 726−734]. Here we present circular dichroism (CD), ^{1}H NMR, analytical ultracentrifugation, and stopped-flow kinetic data to better define the quaternary structure of hemoglobins in which the linkage between the proximal histidines and the polypeptide backbone has been broken [Barrick et al. *Nat. Struct. Biol. 4,* 78−83 (1997)] and to characterize the distal ligand binding properties of these proximally detached Hbs. CD spectroscopy indicates that rHb (αH87G) and rHb (αH87G/βH92G) retain at least partial T-quaternary structure with distal ligand bound, whereas rHb (βH92G) does not, consistent with ^{1}H NMR spectra. Analytical ultracentrifugation reveals significant tetramer dissociation in rHb (βH92G) to be the likely cause of loss of T-state markers. These quaternary structure studies indicate that in distally liganded Hb, the T-state is compatible with proximal linkages in the β- but not the α-chains. ^{1}H NMR titrations of rHb (αH87G) with *n*-butyl isocyanide demonstrate the α-chains to be of high affinity as compared with the β-chains. Comparing ligand association and dissociation rates between the rHb (αH87G) variant with the T- and R-states of wild-type Hb A indicates that at the α-chains, carbon monoxide affinity is modulated entirely by the proximal linkage, rather than from distal interactions. Some residual allosteric interactions may remain operative at the β-chains of rHb (αH87G).

Human normal adult hemoglobin (Hb A)[1] displays a range of complex binding and linkage phenomena that are critical to its function (*1*−*4*). Through careful structural analysis (*5*, *6*) and through mutagenesis, thermodynamic, kinetic, and spectroscopic studies, many of the amino acid residues that play key roles in allostery and cooperativity are being identified, and an understanding of how these residues influence energetic and kinetic processes that relate to cooperativity and allostery is emerging (*7*−*22*). One pair of residues in hemoblogin that have largely escaped site-directed mutagenesis, because of their presumed central role in organizing the structure of the heme pockets, is the proximal histidines. The proximal histidines are directly bonded to the heme irons, and thus connect, through a bonding network, the reactive heme sites to the polypeptide backbone.

These proximal histidine linkages have been proposed by Perutz and others to play a critical role in the cooperativity of ligand binding in wild-type Hb A (*5*, *6*, *23*−*25*). The proximal linkages are proposed to mechanically couple distal ligand binding to the overall quaternary structure of the protein, producing in a change in quaternary structure from T to R in response to distal ligand binding. Indeed, coupling of the proximal environment to the subunit interfaces has been suggested from studies by Morishima and co-workers on chimeric hemoglobins in which sequence blocks in the proximal pocket are substituted (*22*). For the T-to-R quaternary structure transition to produce cooperativity, the reactivity of the unoccupied heme sites must increase in the R-state. This enhancement of distal ligand reactivity in the R-state may result from the same mechanical linkage that initiates the T-to-R transition, namely, the proximal histidine−polypeptide linkage. Alternatively, enhanced reactivity in the R-state may result from structural changes in the residues that surround the distal ligand binding site (*25*).

Comparison of crystal structures of T- and R-state Hbs show structural changes on the distal faces of the heme that could be plausible sources of enhanced R-state distal ligand affinity, especially at the β-chains. Several site-directed mutagenesis studies of both Hb and myoglobin (Mb) have

† Supported by a research grant from the NIH (HL-24258) to C.H., and from a Scientist Development Grant from the American Heart Association (9930126-N) to D.B.

* To whom correspondence should be addressed.

‡ T. C. Jenkins Department of Biophysics, Johns Hopkins University, 3400 North Charles St., Baltimore MD 21218.

§ Department of Biological Sciences, Carnegie Mellon University, 4400 Fifth Avenue, Pittsburgh PA 15213-2683.

[1] Abbreviations: Hb, hemoglobin; Mb, myoglobin; Hb A, normal adult hemoglobin; rHb, recombinant hemoglobin produced in *E. coli*; HbCO, carbonmonoxyhemoglobin; imd, imidazole; ^{1}H NMR, proton nuclear magnetic resonance; CD, circular dichroism; IHP, inositol hexaphosphate; *n*-buNC, *n*-butyl isocyanide; PP, protoporphyrin IX.

10.1021/bi002165q CCC: $20.00
Published on Web 03/13/2001

shown that residues in the distal pocket greatly influence equilibrium and kinetics of distal ligand binding (*7*, *8*, *12*, *15*). The increased distal ligand affinity of the R-state may instead result from changes in the heme and proximal histidine, which include heme flattening, movement of the iron toward the distal face of the heme, and coincident movement of the proximal histidine (*5*). Increased steric accessibility of the iron is expected to increase distal ligand affinity, and several studies of the reactivity of heme-methylimidazole complexes in solution support these expectations. The interaction between the sterically hindered 2-methylimidazole and five-coordinate ferrous heme in organic solvents is weak as compared with unhindered imidazoles, presumably by steric clash between the methyl group and the heme (*26*−*28*). As a result, the affinity of distal ligands such as CO and O_2 for heme complexed with 2-methylimidazole is low (*28*, *29*), consistent with crystallographically observed lengthening of the Fe-O_2 bond seen in the crystal structure of O_2-heme complexed with 2-methylimidazole as compared with the unhindered 1-methylimidazole.

The studies presented here are designed to further our understanding of the structural origins of cooperativity and allostery in Hb A. We have produced three recombinant hemoglobins (rHbs) in which the covalent bonds between the proximal histidines and the polypeptides are severed. We have replaced the proximal histidines of the α-chains and/or β-chains with glycine and have added imidazole (imd) in trans to mimic the local bonding interactions of the proximal histidines in the absence of their normal covalent linkages to the polypeptide (*17*). We designate these three recombinant proteins rHb (αH87G), in which we have severed linkages in the α-chains only, rHb (βH92G), in which we have severed linkages in the β-chains only, and rHb (αH87G/βH92G), in which we have severed linkages in both α- and β-chains. The Perutz model for cooperativity predicts that proximal detachment should prevent quaternary structure switching, i.e., T-state structure should persist after saturation with distal ligand. As a result, cooperativity is predicted to be lost. Distal ligand affinity in this predicted noncooperative, detached T-state tetramer will depend on the degree to which affinity is controlled by the proximal versus distal mechanisms. If distal ligand affinity is controlled largely through the proximal linkage mechanism, affinity should be nearly as high as in R-state hemoglobin, even though the proximally detached protein remains in the T-state. If, however, distal ligand affinity is controlled largely through distal interactions that change between T and R, the affinity should be closer to that of T-state hemoglobin. A mixture of the two mechanisms should give rise to distal ligand affinity that is between T- and R-state levels.

We have shown previously that severing the proximal linkage, which we refer to as "proximal detachment", increases distal ligand affinity and decreases cooperativity, consistent with the Perutz mechanism (*17*). In addition, we have shown that proximal detachment causes partial retention of T-state markers in the ^{1}H NMR spectrum of two of our three proximally detached proteins with distal ligand bound (*17*), suggesting that proximal detachment uncouples quaternary structure from distal ligand binding, leaving these detached Hbs in the T-state. If indeed these proximally detached Hbs are stuck in the T-state, they can be used to evaluate the extent to which proximal versus distal mechanisms contribute to distal ligand affinity enhancement in the R-state.

Here, the quaternary structure of our proximally detached rHbs is analyzed by circular dichroism (CD) spectroscopy, ^{1}H NMR, and by analytical ultracentrifugation to better characterize the structural consequences of rupturing this potentially critical proximal control mechanism. ^{1}H NMR and stopped flow absorbance are used to analyze the relative reactivity of proximally detached distal ligand binding sites to provide a more quantitative assessment of the proximal mechanism in allosteric control and to learn how this control is kinetically partitioned. We find that for the distal ligand CO, proximal detachment in the α-subunit increases reactivity to a level near to that for the R-state of wild-type Hb A, despite the persistence of T-state structure. This affinity enhancement appears to be partitioned into both an enhanced CO on-rate and a decreased CO off-rate as compared to the T-state of wild-type Hb A. For a bulkier distal ligand, *n*-butyl isocyanide (*n*-buNC), residual allosteric interactions appear to modulate reactivity.

MATERIALS AND METHODS

Protein Purification. Proximally detached hemoglobins were produced using an *E. coli* expression vector containing both the human α- and β-globin genes (*30*). Protein was expressed and purified as described (*17*, *30*). Imidazole was maintained at a concentration of 10 mM at all stages of expression and purification to ensure saturation of proximal ligand sites.

Circular Dichroism Spectropolarimetry. All CD samples contained 0.1 M sodium phosphate, pH 7.2, and 10 mM imd. Deoxy-Hb was prepared by first flushing samples with O_2 for 1 h on ice, under direct illumination from a halogen lamp to exchange tightly bound CO that is present during purification and long-term storage. Bound O_2 was then removed by flushing with nitrogen for an hour, and deoxy-Hb samples were transferred anaerobically to sealed 0.1-cm stress-free quartz cells. The cuvettes contained 0.3 μL of a solution of 1 M sodium dithionite that had been anaerobically prepared. To prepare CO-saturated samples, protein samples and cuvettes were flushed with CO prior to transfer. Concentrations ranged from 0.56 to 0.92 mM in hemes, as determined from visible absorbance spectra and published extinction coefficients (*2*). CD spectra were collected on a Jasco J-715 spectropolarimeter at 25 °C. CD was scanned at a rate of 5 nm/min with a bandwidth of 1 nm, and nine consecutive scans were averaged for each spectrum.

Analytical Ultracentrifugation. All ultracentrifugation samples contained 0.1 M sodium phosphate, 10 mM imd, and 1 mM EDTA, and had a pH of 7. Samples were deoxygenated in stoppered vials by blowing a gentle stream of CO over each sample while stirring. Anaerobically prepared sodium dithionite was added to each sample to a concentration of 5 mM, and samples were loaded into velocity ultracentrifugation cells in an anaerobic chamber. Samples were 80 μM in hemes. Velocity sedimentation experiments were run on a Beckman XLA/XLI analytical ultracentrifuge spinning at 45 000 rpm, at 25 °C. Radial distribution profiles were obtained by measuring absorbance at 500 nm, a minimum of absorbance for HbCO. Data were

analyzed using the program "Svedberg" (*31*, *32*). A modified Fujita-MacCosham function was used to determine the sedimentation and diffusion coefficients for each HbCO sample.

^{1}H NMR. All ^{1}H NMR samples contained 0.1 M sodium phosphate, pH 7.2, and 10 mM imd. Proteins were concentrated to around 5 wt % (approximately 0.7 mM tetramer) unless otherwise noted. HbCO and deoxy-Hb samples were prepared as described above and were transferred anaerobically to sealed NMR tubes under positive pressure. To avoid met-Hb formation, all deoxygenated samples were made 10 mM in deoxygenated sodium dithionite. Inositol hexaphosphate (IHP) was purchased as a dipotassium salt from Sigma Chemical Company (St. Louis, MO) and was neutralized with NaOH. *n*-butyl isocyanide (*n*-buNC) was purchased from Aldrich Chemical Co. (Milwaukee, WI) and was dissolved in deoxygenated water to a concentration of 0.1 M.

^{1}H NMR spectra were collected at 300-MHz on a Bruker AM-300 spectrometer. Water suppression was achieved using a jump-return pulse sequence (*33*). For deoxy-Hb spectra, 16 384 FIDs were averaged, each containing 8k complex points, and 71.4 kHz sweep-width. For HbCO spectra, 1024 FIDs were averaged, each containing 8k complex points, and 8 kHz sweep-widths. Proton chemical shifts are referenced to the water resonance, which occurs 4.76 ppm downfield from the methyl proton resonance of 2,2-dimethyl-2-silapentane-5-sulfonate at 29 °C.

Measurement of Rates of CO Association and Dissociation. Progress curves for CO binding and dissociation were determined by stopped-flow methods using an Olis stopped-flow apparatus (Bogart, Georgia). The dead-time of the instrument was around 3 ms. Binding and dissociation of CO was determined by measuring absorbance changes of the heme chromophore. Proteins were buffered at pH 7.0 using 0.1 M sodium phosphate and contained 10 mM imd. Buffers were purged extensively with argon to remove traces of oxygen. All reactions were measured at 20 °C.

For determination of CO binding rates, deoxy-Hb was prepared as described above. Sodium dithionite that had been prepared anaerobically was added to 5 mM prior to mixing to keep the solutions O_2-free and to keep the heme irons in the ferrous oxidation state. To initiate the CO binding reaction, deoxy-Hb solutions were mixed with equal volumes of buffer containing CO. To prepare buffers with subsaturating CO concentrations, a 10-mL glass syringe fitted with a three-way stainless steel stopcock and containing an 0.8-cm magnetic stir-bar was purged with nitrogen and was then rinsed with and finally filled with CO-saturated buffer. All gas bubbles were expelled, as was part of the CO-saturated buffer. The syringe was then topped up, using anaerobic methods, with argon-saturated buffer, and the solution was mixed using the magnetic stir-bar. This process was repeated to further dilute the CO. In some cases, the reverse procedure was used, i.e., the syringe was filled with argon-saturated buffer, and a small volume of CO-saturated buffer was added. Both procedures yielded similar results.

To measure CO dissociation, HbCO was mixed with buffer of identical composition that had been saturated with NO. For CO dissociation reactions, sodium dithionite was omitted as it was found to react with the dissolved NO. Because NO binding to Hb is fast and nearly irreversible, the rate of replacement of CO by NO is limited by CO dissociation (*2*, *34*, *35*). Thus, the rate of CO dissociation can be determined by measuring the progress of the CO−NO substitution reaction.

Progress curves for CO dissociation were fitted using nonlinear least-squares by single exponentials of the form

$$A(t) = \Delta A e^{-kt} + A_\infty \quad (1)$$

or by a pair of exponentials of the form

$$A(t) = \Delta A_1 e^{-k_1 t} + \Delta A_2 e^{-k_2 t} + A_\infty \quad (2)$$

In these equations, A_∞ represents the final absorbance value after the reaction has gone to completion, and ΔA_i represents the difference in absorbance between the start- and end-points of the reaction (eq 1) or one of the two the kinetic phases (eq 2).

For CO binding reactions, progress curves were fitted using several models. At saturating (500 μM) CO concentrations, CO was in 50-fold excess at the start of the reaction, so an integrated rate expression in which CO concentration is held constant was fitted to the data. Both single and double exponentials were fitted, as described above. At lower concentrations of CO, this approximation could not be used. Instead, a simple bimolecular model was adopted of the form

$$\mathrm{Hb} + \mathrm{CO} \xrightarrow{k_{bi}} \mathrm{HbCO}$$

The rate law for the above scheme can be written as

$$\frac{d[\mathrm{Hb}]}{dt} = -k_{bi}[\mathrm{Hb}][\mathrm{CO}] = -k_{bi}([\mathrm{Hb}]^2 + [\mathrm{Hb}]([\mathrm{CO}]_0 - [\mathrm{Hb}]_0)) \quad (3)$$

where the subscripts 0 are used to designate concentrations at the start of the reaction. Equation 3 is separable, and can be integrated to yield

$$[\mathrm{Hb}] = \frac{[\mathrm{Hb}]_0([\mathrm{CO}]_0 - [\mathrm{Hb}]_0)}{[\mathrm{CO}]_0 \exp\{k_{bi}([\mathrm{CO}]_0 - [\mathrm{Hb}]_0)t\} - [Hb]_0} \quad (4)$$

Equation 4 can then be used to give the change in absorbance as a function of time:

$$A(t) = \Delta A\left\{\frac{[\mathrm{CO}]_0 - [\mathrm{Hb}]_0}{[\mathrm{CO}]_0 \exp^{k_{bi}t([\mathrm{CO}]_0 - [\mathrm{Hb}]_0)} - [\mathrm{Hb}]_0}\right\} + A_{\mathrm{HbCO}} \quad (5)$$

Equation 5 can be considered to have four adjustable parameters in addition to the second-order association rate constant: the starting concentrations of Hb and CO, the absorbance of HbCO, and ΔA (the difference in absorbance between deoxy-Hb and HbCO). Since the goal of the fitting procedure is to determine k_{bi} accurately (and to determine whether the model is consistent with the data), the other four parameters were fixed at their estimated concentration and absorbance values. However, it was found that at some starting CO concentrations, subsets of these parameters were well-determined by the progress curves, and allowing adjustment of such parameters during fitting significantly improved agreement between the model and the data. For example, at

low CO concentration, $[CO]_0$ was well determined by the data, whereas A_{HbCO} was not. Therefore, in this fitting, A_{HbCO} was fixed at a value determined from the end of a progress curve at saturating CO, and $[CO]_0$ was optimized during the fit. At higher [CO], the reverse was true: A_{HbCO} was well determined by the progress curves and was optimized during the fit, whereas $[CO]_0$ was not well-determined and was fixed at its experimentally predetermined value.

For CO binding to rHb (αH87G), eq 5 was fitted to progress curves obtained at low concentrations of CO (where CO concentration was less than or equal to total heme concentration) to estimate the second-order rate constant associated with the fast phase. To determine the rate constant of the slow phase, a simple single exponential (eq 1) was fitted to progress curves obtained at saturating CO concentrations. At intermediate CO concentrations where both phases are seen, neither eq 1 nor eq 5 could not be used.

RESULTS

Near-UV Circular Dichroism on Proximally Detached HbCOs. CD spectroscopy has been shown to provide a valuable assessment of the quaternary structure of Hb A (*9*, *36*−*38*). Although the CD spectrum of hemoglobin is dominated by heme transitions, which are largely dependent on distal ligand binding rather than quaternary structure, the region of the spectrum containing signals from the aromatic side chains contains a transition that has been shown to depend on quaternary structure rather than heme ligation (*36*, *37*). It has been suggested that this transition, a peak of negative ellipticity centered at 287 nm in T-state deoxy-Hb which is largely absent in R-state HbO_2 and HbCO, results from a tryptophan (*β*W37) or a tyrosine (αY42) in the $\alpha_1\beta_2$ subunit interface.

CD spectra of the CO forms of the proximally detached Hbs were collected and compared with spectra of wild-type Hb A in the CO (R) and deoxy (T) forms (Figure 1). Spectra of wild-type deoxy-Hb A and HbCO A collected here closely resemble those of oxy- and deoxy-Hb A published previously, both in shape and in magnitude [compare with Figure 3 of ref *36*]. The two prominent bands in the wild-type HbCO A spectrum, located at 259 and 343 nm, are both greatly enhanced as compared to deoxy Hb A (Figure 1, panel A). These two bands have been suggested to result from the heme chromophore and thus report directly on ligand−heme interactions rather than rearrangement of the protein. In support of this, enhancement of both of these bands is also seen in carbonmonoxy-myoglobin (MbCO) as compared to deoxy-Mb (Figure 1, panel E), which lacks quaternary structure and undergoes minimal tertiary structure change upon distal ligand binding. In contrast, the negative band at 287 nm in the CD spectrum of deoxy-Hb is absent in the spectrum of deoxy-Mb, consistent with its reporting on specific quaternary interactions within the T structure.

CD spectra of proximally detached HbCOs have features of both wild-type HbCO A and deoxy-Hb A spectra (Figure 1, panels B−D, Table 1). In particular, for rHbCO (αH87G) and rHbCO (αH87G/*β*H92G), although the bands at 259 and 343 nm (those indicative of distal ligand binding to heme) show enhanced ellipticity, similar to the enhancement seen in the spectrum of wild-type HbCO A, the quaternary structure band at 287 nm retains substantial negative ellipticity, reminiscent of the spectrum of wild-type deoxy (T)

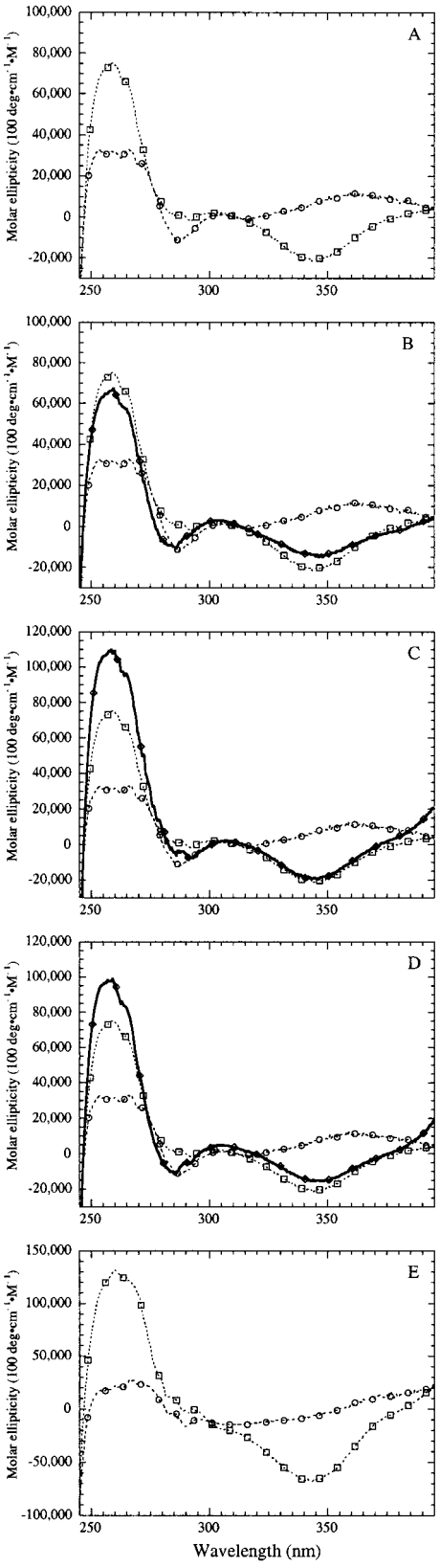

FIGURE 1: Near-UV circular dichroism spectra of proximally detached carbonmonoxy hemoglobins. (A) Wild-type deoxy-Hb A and HbCO (circles and squares, respectively). The negative ellipticity at 287 nm has been attributed to the *β*37 trp in the T-quaternary structure by Simon and Cantor (*36*). (B) rHbCO (αH87G), (C) rHbCO (*β*H92G), and (D) rHbCO (αH87G/*β*H92G), (thick lines with diamonds), each plotted with wild-type deoxy-Hb A and HbCO as in panel (A). (E) Horse myoglobin in the deoxy- (circles) and CO-forms (squares). Conditions: 0.1 M sodium phosphate, 10 mM imd, 1.5 mM sodium dithionite, pH 7.2, 25 °C.

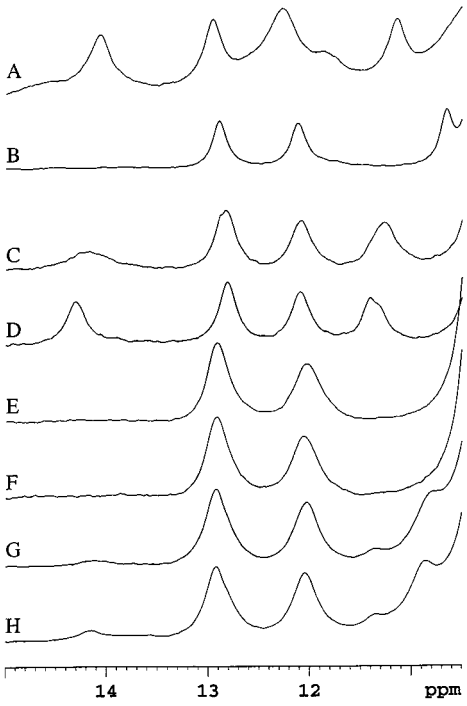

FIGURE 2: The effect of IHP on the ^{1}H NMR spectra of proximally detached carbonmonoxy hemoglobins. 300 MHz proton ^{1}H NMR spectra for wild-type deoxy-Hb A (A); wild-type HbCO (B); rHbCO (αH87G) (C, D); rHbCO (βH92G) (E, F); rHbCO (αH87G/βH92G) (G, H). Conditions: 0.1 M sodium phosphate, 10 mM imd, 10 mM sodium dithionite, pH 7.2, 29 °C; samples D, F, and H contain 10 mM IHP.

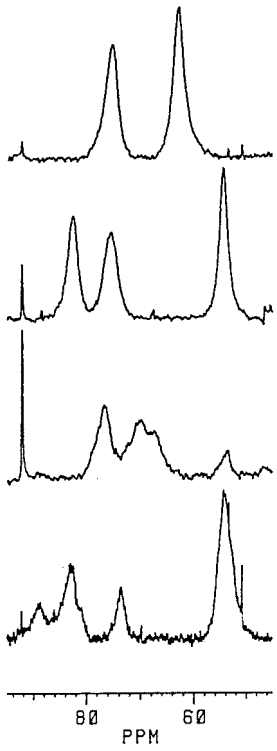

FIGURE 3: ^{1}H NMR spectra of proximally detached deoxy-hemoglobins. 300 MHz proton ^{1}H NMR spectra for wild-type deoxy-Hb A (top), rHb (αH87G) (second from top), rHb (βH92G) (third from top), and rHb (αH87G/βH92G) (bottom) deoxy-Hbs in the presence of 10 mM imd. Resonances in this region are from protons in close proximity to the unpaired electrons of the heme irons. For wild-type Hb A, the resonances at 63.3 and 75.8 ppm have been assigned to the Nδ Hs of the α- and β-chain proximal histidines, respectively (*45*, *46*). Conditions: 0.1 M sodium phosphate, 10 mM imd, 10 mM sodium dithionite, pH 7.2, 29 °C.

Hb A (Figure 1, panels B and D). The CD spectrum of rHbCO (βH92G) shows less negative ellipticity in this region (280−290 nm), resembling the spectrum of wild-type HbCO A (Figure 1, panel C). On the basis of CD in the region of the T-state marker, it appears that rHbCO (αH87G) and rHbCO (αH87G/βH92G) HbCOs have significant T-quaternary structure in the vicinity of the reporting side chains, whereas rHbCO (βH92G) lacks this structure.

Analytical Ultracentrifugation. To gain qualitative information on the tetramer stability of the proximally detached Hbs, we have used velocity sedimentation to determine sedimentation coefficients for the CO forms of the detached Hbs. We have used the CO forms of these proteins because for wild-type Hb, the tetrameric deoxy form is very stable, rendering sedimentation studies relatively insensitive to changes in dimer−tetramer stability. Because of linkage of the quaternary structure to distal ligand binding, the addition of CO weakens the tetramer, aiding in detection of tetramer−dimer equilibrium (*39*).

Velocity sedimentation of wild-type and proximally detached HbCOs indicate that the sedimentation coefficient for rHbCO (αH87G) is the same, within error, as that obtained for wild-type HbCO A (about 4.1 S, Table 2) and is similar to published values wild-type HbCO A (*40*−*42*). However, the sedimentation coefficients for rHbCO (αH87G/βH92G) and rHbCO (βH92G) are significantly smaller (3.5 and 2.8, respectively). These numerical values suggest that although wild-type and rHbCO (αH87G) are fully associated, or are at least associated to the same degree, rHbCO (αH87G/βH92G) and rHbCO (βH92G) are partly dissociated. Calculated diffusion coefficients support partial dissociation for rHbCO (αH87G/βH92G) and rHbCO (βH92G): whereas diffusion coefficients for wild-type HbCO A and rHbCO (αH87G) are nearly identical (8.0−8.1 × 10^{-7} cm^2 s^{-1}), that for rHbCO (αH87G/βH92G) is larger (8.6 × 10^{-7} cm^2 s^{-1}), and that for rHbCO (βH92G) is larger still (9.0 × 10^{-7} cm^2 s^{-1}), suggesting a decrease in Stokes' radius for these two

Table 1: Molar Ellipticities of Proximally Detached Hemoglobins at Selected Wavelengths[a]

protein	$[\theta]_{287}$	$[\theta]_{259}$	$[\theta]_{343.5}$
wild-type Deoxy-Hb A	−12 100	+31 100	+6 800
wild-type HbCO A	+1 000	+75 200	−21 700
rHbCO (αH87G)	−8 300	+66 600	−13 800
rHbCO (βH92G)	−3 700	+108 000	−19 300
rHbCO (αH87G/βH92G)	−8 900	+98 900	−15 400

[a] Molar ellipticities are reported in deg cm^{-1} M^{-1} × 10^{-2}, where the molar concentration refers to moles of heme per liter, rather than moles of hemoglobin tetramer. Uncertainties in molar ellipticity values are around 1200 deg cm^{-1} M^{-1} × 10^{-2} at the 67% confidence level.

Table 2: Sedimentation and Diffusion Coefficients of Proximally Detached Carbonmonoxyhemoglobins

protein	S[a]	D[b]
wild-type HbCO	4.05	8.08
rHbCO (αH87G)	4.11, 4.17	8.04
rHbCO (βH92G)	2.81	9.01
rHbCO (αH87G/βH92G)	3.51	8.64

[a] In Svedbergs (10^{-13} seconds). [b] In Ficks (10^{-7} cm^2 s^{-1}), both determined using the modified Fujita-MacCosham function from the program SVEDBERG *(31, 32)*.

detached HbCOs. These results are consistent with equilibrium ultracentrifugation experiments (results not shown) in which rHbCO (αH87G) and wild-type HbCO A are nearly identical in their radial distribution profiles, but rHbCO (*β*H92G) and, to a lesser extent, rHbCO (αH87G/*β*H92G) distribute as lower molecular weight complexes.

Effects of IHP on T-State Markers in the ^{1}H NMR Spectra of Proximally Detached HbCOs. There are several resonances in the ^{1}H NMR spectrum of wild-type Hb A that are sensitive indicators of Hb quaternary structure. Resonances at 14.1 and 11.2 ppm in the ^{1}H NMR spectrum of wild-type deoxy-Hb A have been assigned to hydrogen bonds (between α42Tyr and *β*99Asp, and between α94Asp and *β*37Trp, respectively) that are formed in the T-quaternary structure, and thus serve as excellent markers for T-state structure (*43*−*47*). When CO is added to wild-type Hb A, these resonances disappear because the R quaternary structure is adopted. We have previously shown that these T-state markers persist in the ^{1}H NMR spectrum of the CO forms of rHb (αH87G) and to a lesser extent the CO form of rHb (αH87G/*β*H92G) (*17*; also see Figure 2). We have also shown that IHP, an allosteric effector that binds to the T-structure of wild-type Hb and thus decreases distal ligand affinity (*48*), also decreases distal ligand affinity in proximally detached Hbs (*17*). Here, we use ^{1}H NMR spectroscopy to test whether the effect of IHP on distal ligand affinity in proximally detached rHbs is a result of enhancement of the stability of the T-state. If this is the case, the T-state markers in the ^{1}H NMR spectra of our proximally detached HbCOs should become more intense upon addition of IHP. For the 14.1 ppm peak in the ^{1}H NMR spectrum of rHbCO (αH87G), this is the case: the 14.1 ppm resonance sharpens and appears to increase in intensity at 10 mM IHP (Figure 2). For rHbCO (αH87G/*β*H92G), there also appears to be some sharpening of the ∼14.1 ppm peak, although the effect is more modest than for rHbCO (αH87G). For both rHbCO (αH87G) and rHbCO (αH87G/*β*H92G), these spectral changes appear to be complete at 2 mM IHP, the lowest concentration that we have examined (data not shown). For rHbCO (*β*H92G), the 14.1 ppm T-state marker is absent at all concentrations of IHP. IHP has less of an effect on the intensity of the T-state marker in the 11.2 ppm region of the spectra of proximally detached HbCOs. For rHbCO (αH87G), the intensity of the ∼11.2 ppm T-state marker does not change, but the frequency of this resonance appears to shift to slightly lower field and has a somewhat asymmetric shape. The observation that the 11.2 ppm T-state marker is insensitive to IHP is not surprising, since it appears to be at approximately full intensity (as compared to the 12.2 and 12.9 ppm resonances) in the absence of IHP. For rHbCO (αH87G/*β*H92G), the weak resonance in this region, which centered at about 11.3 ppm, shows neither intensity or chemical shift sensitivity to IHP. rHbCO (*β*H92G) lacks this T-state marker in both the absence and presence of IHP.

Hyperfine-Shifted Resonances in the ^{1}H NMR Spectra of Proximally Detached Deoxy-Hbs. In the ^{1}H NMR spectrum of deoxy-Hb, two resonances have been identified at very low frequencies. Their low chemical shifts result from hyperfine interactions (either contact or dipolar) with the unpaired electrons of the high-spin deoxy-heme irons. These resonances, at 63.3 and 75.8 ppm, have been assigned to the Nδ*H*s of the α and *β*-chain proximal histidines, respectively (*49*−*51*). Because these resonances originate at the heme pocket of each subunit and are baseline-resolved, they are excellent probes for resolving ligand binding to the α- versus *β*-chain hemes (*22*, *51*−*53*). Resolving distal ligand binding curves into binding at the α- versus *β*-chains is of particular interest for rHb (αH87G), where analysis of absorbance-monitored distal ligand binding curves yield a Hill coefficient of less than one. As absorbance spectroscopy cannot distinguish between ligand binding at the α- and *β*-chains, the molecular origin of the shallow rHb (αH87G) distal ligand binding curve (negative cooperativity versus affinity differences between α- and *β*-chains) remains uncertain.

The low-field ^{1}H NMR spectra of wild-type deoxy-Hb A and proximally detached deoxy-rHbs are shown in Figure 3. Unlike the two baseline-resolved resonances seen in the spectrum of wild-type Hb A, the proximally detached spectra show extra resonances. In addition, peak positions shift significantly between wild-type Hb A and the three proximally detached Hbs, preventing transference of assignments from wild-type deoxy-Hb A.

One potential source of extra peaks as a result of proximal detachment is that, as compared with proximal histidine ligands, proximal imd ligands will have an extra hydrogen attached to the carbon analogous to the histidine C*γ*. If the proximal imd ligand binds to the heme without significant tilt, the through-bond and through-space relationship between the electrons of the heme iron and the C*γ*H should be similar to those between the electrons of the heme iron and the Nδ*H*.[2] Thus, the C*γ*H may be expected to resonate at approximately the same frequency as the Nδ*H*. Such behavior is observed for proximally detached sperm whale deoxy-Mb. As compared with wild-type deoxy-Mb, which has a single proximal Nδ*H* resonance at around 76 ppm (Figure 4, panel A), H93G deoxy-Mb has two resonances of similar intensity, one at 82 ppm and one at 58 ppm (Figure 4, panel D). By replacing the H_2O with D_2O, the 76 ppm resonance of wild-type deoxy-Mb is eliminated (compare Figure 4, panels A and C), confirming the assignment of this resonance to the labile the Nδ proton (*50*). For H93G deoxy-Mb, replacement of H_2O with D_2O eliminates the 82 ppm resonance (Figure 4, panel F), suggesting that the 82 ppm resonance results from a labile proton, presumably the imd NH, and that the 58 ppm resonance results from the imd Cδ*H*. To confirm that the resonance of the nonlabile proton at 58 ppm is attached to an imd carbon, the imd in the H93G deoxy-Mb sample was replaced with fully deuterated (d_4-) imd. Since the sample was prepared in H_2O, the labile imd Nδ*D* is expected to be replaced with an H; however, the three carbon-borne deuterons of the d_4-imd are nonlabile and should be retained in complex with H93G Mb. The result of imd deuteration is that the resonance at 58 ppm disappears from the spectrum (compare Figure 4, panels D

[2] The nomenclature that we use here to specify positions on the proximal imidazole parallels that used to specify atom positions in proximal histidine (Nϵ coordinating the iron, Nδ*H* in opposition). Using IUPAC nomenclature, Nϵ would be designated N3, Nδ*H* would be designated N1H, and the three ring CHs would succesively be designated C2, C4, and C5. Although in solution C4 and C5 are not distinguishable because of tautomerization of N1H and N3, when bound to the asymmetric proximal pocket, C4 and C5 become chemically distinct.

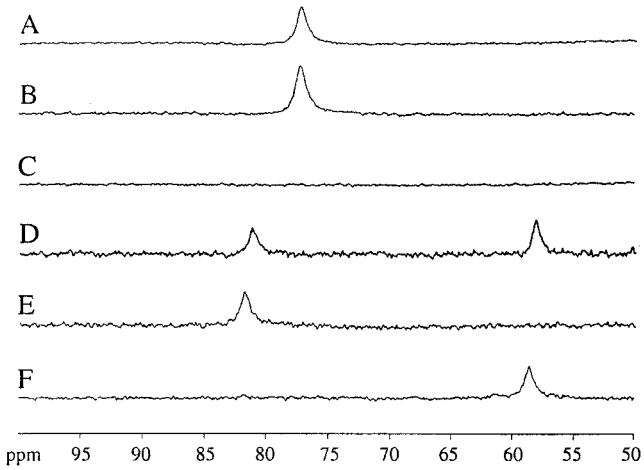

FIGURE 4: 300 MHz ^{1}H NMR spectra of wild-type and proximally detached sperm whale deoxy-myoglobins. (A) Wild-type deoxy-Mb, (B) wild-type deoxy-Mb with 10 mM imd, (C) wild-type deoxy-Mb in D_2O, (D) H93G deoxy-Mb with 10 mM imidazole, (E) H93G deoxy-Mb with 10 mM deuterated (d4-) imd, (F) H93G deoxy-Mb with 10 mM imidazole in D_2O. Conditions: 0.1 M sodium pyrophoshpate, pH 8.6, 25 °C.

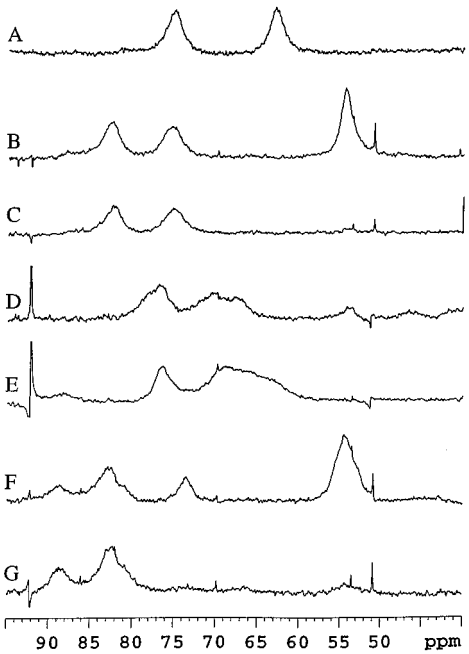

FIGURE 5: Assignment of hyperfine-shifted resonances to nonexchangeable imidazole protons. 300-MHz spectra of proximally detached Hbs with either imd or perdeuterated (d_4-) imd. (A) wild-type Hb A, (B) rHb (αH87G) with 10 mM imd, (C) rHb (αH87G) with 200 mM d_4-imd, (D) rHb (βH92G) with 10 mM imd, (E) rHb (βH92G) with 200 mM d_4-imd, (F) rHb (αH87G/βH92G) with 10 mM imd, (G) rHb (αH87G/ βH92G) with 200 mM d_4-imd. Conditions: 0.1 M sodium phosphate, 10 mM sodium dithionite, pH 7.2, 29 °C.

and E), confirming that this resonance derives from a proton bound to an imd carbon, presumably that equivalent to the Cγ of the proximal histidine (which, in histidine, is not directly bonded to a proton).

To assign proximal imd and histidine resonances in the proximally detached Hbs, imd was replaced with deuterated imd (Figure 5). For rHb (αH87G) complexed with deuterated imd, the resonance at 54 ppm is lost, while the two downfield resonances are retained. This result demonstrates that the 54 ppm resonance comes from an imd carbon-bound proton, presumably at the Cγ position, and suggests that the two downfield resonances come from proximal NδHs, presumably one from imds at the α-chains and one from the proximal histidines of the β-chains (βH92). This assignment is qualitatively similar to that for the imd complex of H93G deoxyMb, in which the carbon-borne proton resonates at 57 ppm, and the imd NH proton resonates at 82 ppm. The fact that the chemical shift of one of the downfield proximal resonances (at around 74.5 ppm) is very similar to the resonance assigned to the β-chain proximal histidines in wild-type deoxy-Hb A suggests that in the deoxy-rHb (αH87G) spectrum this resonance may derive from the β-chain proximal histidine (βH92) NδHs, and the farthest downfield resonance (82 ppm) results from the NδH of the imds at the α-chains. For the fully detached deoxy-rHb (αH87G/βH92G), replacement of imd with deuterated imd results in the loss of the resonances at 54 ppm, the same as in the deoxy-rHb (αH87G), and also at 74 ppm. This suggests the resonance at 54 ppm derives from the imd CγHs of the α-chains, and that at 74 ppm derives from the imd CγHs of the β-chains. Two resonances remain in the far-downfield region after substitution with deuterated imd (at 82.5 and 89 ppm). The resonance at 82.5 ppm has a chemical shift similar to the resonance assigned to the NδH of the imd at the α-chains in the spectrum of deoxy-rHb (αH87G) and may result from the same protons in deoxy-Hb (αH87G/βH92G). One puzzling feature of the proximal ^{1}H NMR spectrum of deoxy-rHb (αH87G/βH92G) is the low intensity of the 74 ppm resonance relative to the 54 ppm resonance. If these two resonances derive from imd ring protons, they should have the same intensity. One possibility is that at imd concentrations in the ^{1}H NMR samples (10 mM), the β-chains are not completely saturated with imd. This would be surprising, since measurement of imd affinity to proximally detached H93G deoxy-Mb has yielded a dissociation constant of about 2 μM (*54*). A second possibility is that the imd proximal ligands in the β-chains occupy multiple conformations with different magnetic environments. Consistent with this second possibility, there appear to be additional shoulders in the deoxy-rHb (αH87G/βH92G) spectrum (one upfield of the 54 ppm resonance, one upfield of the 82.5 ppm resonance).

Unlike the downfield ^{1}H NMR spectrum of deoxy-rHb (αH87G), which has a resonance at the same frequency as the β-chain proximal histidine resonance of wild-type Hb A, the spectrum of deoxy-rHb (βH92G) lacks a resonance at the frequency of the α-chain proximal histidine resonance of wild-type deoxy-Hb A. This indicates that proximal detachment in the β-chain has structural consequences at the α-chain heme sites. Further, neither of the potential β-chain imidazole resonances (74 and 89 ppm) of deoxy-rHb (αH87G/βH92G) are visible in the spectrum of deoxy-rHb (βH92G), indicating that the environment at the β-chain heme sites is also different between the two proteins. Replacement of imd with deuterated imd in deoxy-rHb (βH92G) produces decreases in signal intensity in two regions of the spectrum. The resonance at 54 ppm disappears, and signal intensity appears to be lost in the region around 66 ppm. The loss of multiple resonances is again consistent with a multiple conformations for the proximally detached β-chain imds. Conformational multiplicity is also suggested by the presence of at least four distinct resonances in the spectrum of deoxy-

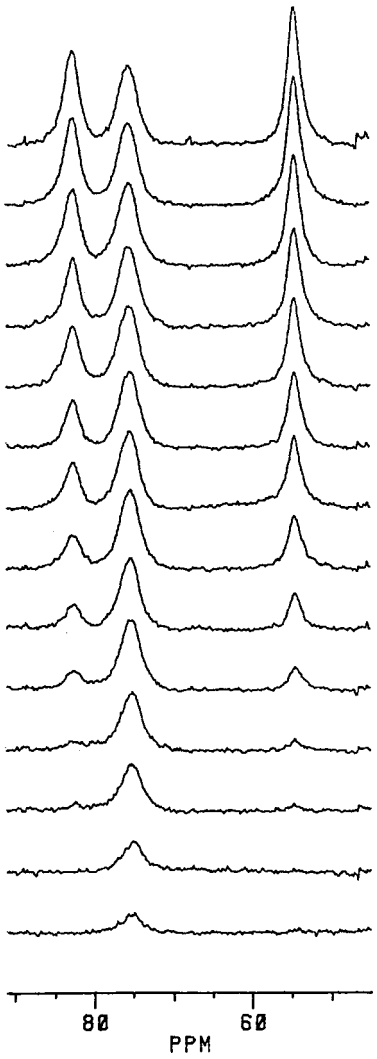

FIGURE 6: Binding of *n*-butyl isocyanide to rHb (αH87G) monitored by ^{1}H NMR. 300-MHz ^{1}H NMR spectra of 1.2 mM rHb (αH87G) (4.85 mM hemes) with increasing concentrations of *n*-butyl isocyanide (n-buNC). From top to bottom: 0, 0.5, 1.0, 1.5, 2.0, 2.5, 3.0, 4.0, 5.5, 7.0, 8.5, 10.0, 13.0, and 16.0 mM total buNC. Conditions: 0.1 M sodium phosphate, 10 mM imd, ~8 mM sodium dithionite, pH 7.2, 29 °C.

rHb (*β*H92G), in contrast with that of deoxy-rHb (αH87G), which shows only three resonances.

Resolution of α- and β-Chain Binding during Titration of rHb (αH87G) with n-buNC. The ability of ^{1}H NMR to resolve signals from the α- and *β*-chain proximal pocket-sallows overall equilibrium distal ligand binding curves to be resolved into microscopic binding events. By titrating deoxy-rHb (αH87G) with *n*-buNC, a distal ligand that binds cooperatively to wild-type Hb A (*55*) but with a stretched isotherm to rHb (αH87G), a clear preference can be seen in the ^{1}H NMR spectrum for *n*-buNC to the α-chains (Figure 6). Addition of limiting amounts of *n*-buNC decrease the intensity of the resonance identified above as resulting from the α-chain imd C*γ*Hs (54 ppm). Concurrent with this loss of intensity, the resonance at 82 ppm also loses intensity, supporting the proposal that this resonance derives from the α-chain. In contrast, the resonance at 74.5 ppm retains its intensity until very high *n*-buNC concentrations (Figure 6). Since the resonance at 82 ppm loses intensity at the same *n*-buNC concentrations as the α-chain imd C*γ*H resonance at 54 ppm and is likely to result from the α-chain imd NH, the remaining 74.5 ppm resonance is likely to be that of the *β*-chain proximal histidine N*δ*Hs. This assignment is consistent with its resonance frequency at 74.5 ppm, which is roughly the same as that of the *β*-chain proximal histidines of wild-type deoxy-Hb A. These results indicate that the low Hill coefficient measured for *n*-buNC binding to rHb (αH87G) by absorbance spectroscopy (*17*) results from heterogeneity between the α- and *β*-chains, rather than from negative cooperativity. Specifically, the α-chains of rHb (αH87G) are of high affinity, whereas the *β*-chains are of low affinity.

CO Dissociation from Proximally Detached Hemoglobins. Equilibrium studies have shown that deleting the covalent bond between the proximal histidines and the F-helices of Hb increases the affinity of O_2 and *n*-buNC, and decreases cooperativity (*17*). To obtain a more complete picture of distal ligand binding to proximally detached Hbs, we have examined the kinetics of CO binding and dissociation. These kinetic studies allow equilibrium changes in affinity to be decomposed into changes in the reactivity of the ligand-free versus ligand-bound forms of the protein. In addition, kinetic measurements of distal ligand binding and dissociation allow direct measurement of reactivity of the T- and R-quaternary structures. Because Hb binds distal ligands cooperatively, isolation of these states is difficult using equilibrium methods, requiring measurements of very high sensitivity and precision (*3*).

Because CO binds to Hb with high affinity, its rate of dissociation cannot be measured by simple ligand dilution. Instead, the rate of dissociation of CO can be measured by competition with NO (*34*, *35*). Because NO combines with Hb much faster than CO, and because NO dissociates very slowly from Hb once bound, mixing HbCO with a saturated solution of NO results in near complete displacement of the CO in a process that is rate limited by CO dissociation (*2*, *34*, *35*). In such exchange experiments, a high level of distal ligand saturation is maintained; thus for wild-type Hb A, the observed kinetics reports on R-state ligand dissociation. However, for the proximally detached Hbs, kinetics should report on ligand dissociation from either the T-state [rHbCO (αH87G)] or from dissociated dimers [rHbCO (*β*H92G)], either with or without proximal restraint. For wild-type HbCO A, rHbCO (*β*H92G), and rHbCO (αH87G/*β*H92G), CO dissociation curves show a single kinetic phase (Figure 7). For rHbCO (αH87G), however, the progress curve clearly reveals two kinetic phases (Figure 7). The biphasic nature of the CO dissociation curve of rHb (αH87G) can also be seen by inspection of residuals: those from fitting a single-exponential decay curve to the CO dissociation data of rHb (αH87G) are highly nonrandom, whereas those from fitting a double exponential are uniformly distributed (Figure 8). In contrast, residuals resulting from fitting single-exponential curves to wild-type Hb A, rHb (*β*H92G), and rHb (αH87G/*β*H92G) CO dissociation curves are all randomly distributed (data not shown). For the two kinetic phases seen for rHb (αH87G), rate constants are separated by around 15-fold, and relative amplitudes for the two kinetic phases are nearly equal (Table 3).

Fitted rate constants for the monophasic CO dissociation curves of rHbCO (*β*H92G) and rHbCO (αH87G/*β*H92G) are only slightly different than that for wild-type HbCO A,

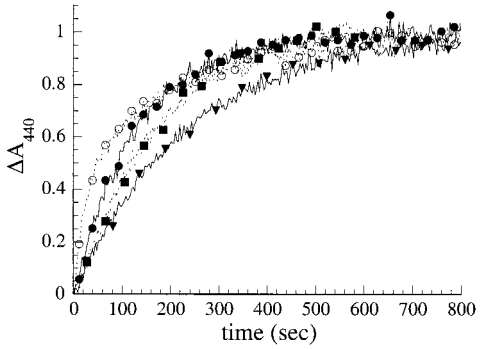

FIGURE 7: Kinetics of CO dissociation from proximally detached hemoglobins by NO competition. Normalized absorbance changes at 440 nm are shown for the replacement of CO with NO from wild-type HbCO A(−▼−), rHbCO (αH87G) (- - -○- - -), rHbCO (βH92G) (−●−), and rHbCO (αH87G/βH92G) (- - -■- - -). Conditions after mixing: 29.2 to 31.5 μM hemes (~7.5 μM tetramers), one-half atmosphere of NO, 0.1 M sodium phosphate, 10 mM imd, 20 °C.

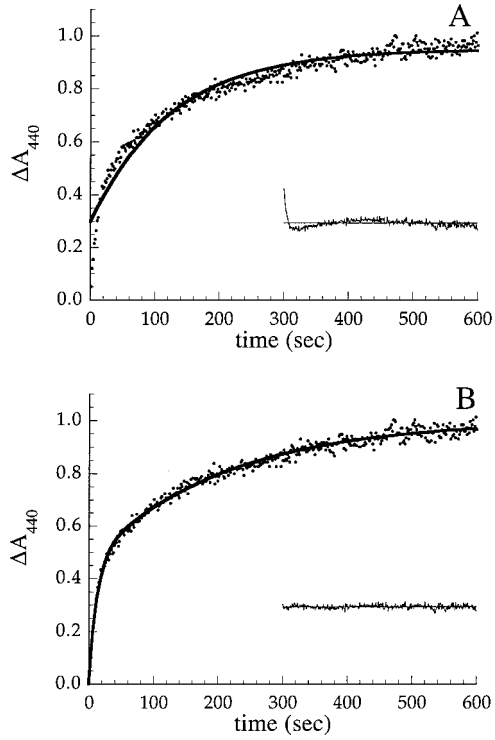

FIGURE 8: Kinetics of CO dissociation from rHbCO (αH87G). Solid lines result from fitting single exponential (panel A) and biexponential (panel B) decay curves to the data (eqs 1 and 2, Materials and Methods). Insets in each panel show residuals from eqs 1 and 2 and are plotted on the same scale for comparison. The solid line represents zero residual. Residuals using the single exponential equation are nonrandom (A), whereas those for the biexponential equation are randomly distributed (B). Conditions are as in Figure 7.

showing an increase of 2- and 1.5-fold, respectively (Table 3). For the biphasic CO dissociation curve of rHbCO (αH87G), the rate constant associated with the fast phase is greater than the overall CO dissociation rate constant for wild-type HbCO A, whereas the slow-phase rate constant for rHbCO (αH87G) the same as the overall dissociation rate constant for wild-type rHbCO A. The addition of IHP has very little effect on the progress curves for CO dissociation from wild-type or rHbCOs (Table 3).

CO Binding to Proximally Detached Hemoglobins. For binding of CO to wild-type deoxy-Hb A, a single-exponential decay curve is observed, and almost all of the reaction can be observed using stopped-flow techniques with saturated CO (500 μM after mixing, Figure 9). However, for the proximally detached deoxy-Hbs, greater than half of the CO binding reaction is completed during the dead-time of the instrument. This missing amplitude is most pronounced for rHb (βH92G) and for rHb (αH87G/βH92G), whereas for rHb (αH87G), the reaction proceeds to around 60% completion in the dead-time (Figure 9). The portion of the progress curve that is detected at 500 μM CO can be fitted reasonably well by a single-exponential decay curve. Fitted second-order rate constants (k_{app}) for CO binding to rHb (βH92G) and for rHb (αH87G/βH92G) are somewhat larger than that for wild-type rHb A by around 5- and 10-fold, respectively (Table 4, k_{app}). Whereas faster overall reaction may explain the missing amplitude for CO binding to rHb (βH92G) and to rHb (αH87G/βH92G), for rHb (αH87G) the apparent second-order rate constant is slightly smaller than for wild-type deoxy-Hb A, that the missing amplitude suggesting results from a second, fast kinetic phase.

To observe the portion of the CO binding curves that are completed in the dead-time in Figure 9, we repeated the stopped-flow measurements at low concentrations of CO. Decreasing CO concentration slows the overall reaction, permitting detection of fast phases. This method allowed Olson and co-workers to characterize the reactivity of the T-state of wild-type Hb A and to characterize the reactivities of a number of variant rHbs (*12*). Progress curves for CO binding to wild-type deoxy-Hb A show a single major kinetic phase (Figure 10, panels A and B). This is most obvious in the plot of the extent of reaction as a logarithmic function time (Figure 10, panel B) at saturating CO concentrations, where a single sigmoidal curve is observed of nearly full amplitude. Fitting a simple bimolecular scheme to progress curves for wild-type Hb A at different CO concentrations yields approximately the same second-order rate constant irrespective of the concentration of CO, and thus, the portion of the curve being fitted (Table 5). Simple progress curves, corresponding to a single major kinetic phase, are also seen for binding of dilute CO to rHb (βH92G) (not shown) and for rHb (αH87G/βH92G) (Figure 10, panels E and F). Saturation is incomplete at substoichiometric CO concentrations, but as CO concentration is increased to exceed the concentration of hemes, the progress curves grow to full saturation. As CO concentration increases, the progress curve becomes more rapid, as expected for a bimolecular reaction, resulting in loss of amplitude to the dead-time of the instrument. For both rHb (βH92G) and rHb (αH87G/βH92G), fitted second-order rate constants are roughly independent of CO concentration at low CO, but at high concentrations the apparent second-order rate constants decrease with increasing CO (Table 5). The origin of this decrease is coincident with the loss of much of the amplitude of the reaction to the dead-time, and may represent a minor, slow kinetic phase. Fitted second-order rate constants for rHb (βH92G) and rHb (αH87G/βH92G) at CO concentrations where the entire progress curve is observed are around 15 to 25 times larger than for CO binding to wild-type deoxy-Hb A.

Table 3: Kinetic Parameters for Carbon Monoxide Dissociation from Proximally Detached Hemoglobins[a]

		single exponential	biexponential fitting			
protein	[IHP] mM	k_{off} 10^{-3} s^{-1}	k_1 10^{-3} s^{-1}	%1	k_2 10^{-3} s^{-1}	%2
wild-type Hb A	0	4.2			nd[c]	
rHb (αH87G)	0	nd[b]	67 (*89*, *45*)	48 (*47*, *48.5*)	5.0 (*5.8*, *4.2*)	52 (*53*, *51.5*)
rHb (αH87G)	1	nd[b]	104	48.5	5.5	51.5
rHb (*β*H92G)	0	8.5 (*10.0*, *7.1*)			nd[c]	
rHb (*β*H92G)	1	9.7			nd[c]	
rHb (αH87G/*β*H92G)	0	6.0			nd[c]	
rHb (αH87G/*β*H92G)	1	5.4			nd[c]	

[a] Although subsequent injections yielded fitted rate constants that differed by less than 10%, larger differences were seen when fresh samples and buffers were prepared and reactions were measured on different days. The results of such measurements (αH87G and *β*H92G) are presented as the mean value, with values from different days given in parentheses. [b] Not determined because progress curves are clearly biexponential. [c] Not determined because progress curves are well fitted using a single exponential.

In contrast to wild-type Hb A, rHb (*β*H92G), and rHb (αH87G/*β*H92G), progress curves for CO binding at low concentration to deoxy-rHb (αH87G) show two kinetically distinct phases (Figure 10, panels C and D). At the lowest CO concentrations, only the fastest phase is detected; the fitted second-order rate constant is as large as that of deoxy-rHb (αH87G/*β*H92G). As the concentration of CO increases, a slower phase becomes evident. These two phases appear to be of approximately equal amplitude (see Figure 10, panel D, 20 *μ*M CO; green dots). As CO concentration increases further, this fast phase disappears, and the progress curve is entirely represented by the slow phase. The fitted rate constant of this phase is slightly smaller than the fitted rate constant for wild-type deoxy-Hb A (Table 5).

The addition of IHP to a final concentration of 1 mM decreases the rate of reaction for wild-type Hb A and all proximally detached rHbs (Table 4).

DISCUSSION

Quaternary Structure. Both the near-UV CD (Figure 1) and ^{1}H NMR studies (Figure 2) show the proximal linkages to be important determinants of quaternary structure, and thus allostery, in Hb A. When the proximal linkages in the α-chains are broken, T-state structural markers persist both in the near-UV CD and ^{1}H NMR spectra when CO is bound as distal ligand. This result suggests that the T-quaternary structure, as defined by the ^{1}H NMR and CD markers, is compatible with *β*-chain proximal restraint [the only type of proximal restraint remaining in rHb (αH87G)]. When the proximal linkages in the *β*-chains are broken, T-state structural markers are diminished (or absent) in the near-UV CD and ^{1}H NMR spectra when CO is bound. This result suggests that the T-quaternary structure is incompatible with α-chain proximal restraint, or that proximal detachment in the *β*-chains favors another quaternary structure. If, unlike the α-chains, proximal restraint in the *β*-chains is not correlated to quaternary structure, then the fully detached rHb (αH87G/*β*H92G) should behave, in terms of quaternary structure, like rHb (αH87G). Instead, the ^{1}H NMR spectrum of rHbCO (αH87G/*β*H92G) shows less T-state character (based on the marker at 14.1 ppm) than is seen in rHbCO (αH87G), but unlike rHbCO (*β*H92G), the resonance is clearly visible. Thus, based on the 14.1 ppm T-state marker, the effects of α- and *β*-chain proximal detachment seem to be opposing. This opposing effect can also be seen in the effect of proximal detachment on hydrodynamic radius (Table 2).

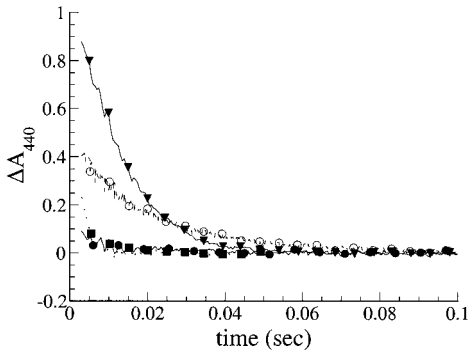

FIGURE 9: Kinetics of CO binding to proximally detached hemoglobins at high CO concentration. Normalized absorbance changes at 440 nm are shown for wild-type deoxy-Hb A (−▼−), deoxy-rHb (αH87G) (- - -○- - -), deoxy-rHb (*β*H92G) (−●−), and deoxy-rHb (αH87G/*β*H92G) (- - -■- - -). Conditions after mixing: 28.5 to 31.5 *μ*M hemes (∼7.5 *μ*M Hb tetramers), one-half atmosphere of CO (0.5 mM), 0.1 M sodium phosphate, 10 mM imd, 2.5 mM sodium dithionite, 20 °C.

The observation that the T-state marker in the near UV CD spectrum of rHbCO (αH87G/*β*H92G) is equal in intensity to that of rHbCO (αH87G) appears to be in conflict with the observation that the 14.1 and 11.2 ppm T-state markers in the ^{1}H NMR spectrum are less intense in rHbCO (αH87G/*β*H92G) than in rHbCO (αH87G). The T-state marker in the near UV CD spectrum is believed to originate from either *β*W37 or αY42 in the $\alpha_1\beta_2$ subunit interface, the same side chains to which the 14.1 and 11.2 ppm T-state markers in the ^{1}H NMR spectrum have been assigned. One possible explanation for this discrepancy between CD and ^{1}H NMR T-state markers is that the diminished intensity of the ^{1}H NMR T-state markers may result from an increased rate of exchange with solvent protons, rather than a significant depopulation of the T-state quaternary structure. Another possible explanation for this discrepancy is that the quaternary structures of wild-type Hb A and of the proximally detached rHbs may not be single "discrete" structures but rather a somewhat plastic family conformations. Such quaternary structure ensembles may be related in overall fold and assembly but may differ in structural and dynamic details to which the various T-state markers are sensitive. Such structural heterogeneity could account for the asymmetric line shape seen in the 12.9 and 11.2 ppm resonances of rHbCO (αH87G) (Figure 2). A dramatic example of structural heterogeneity can be seen by comparing the many different crystal structures of Hb A that have been determined

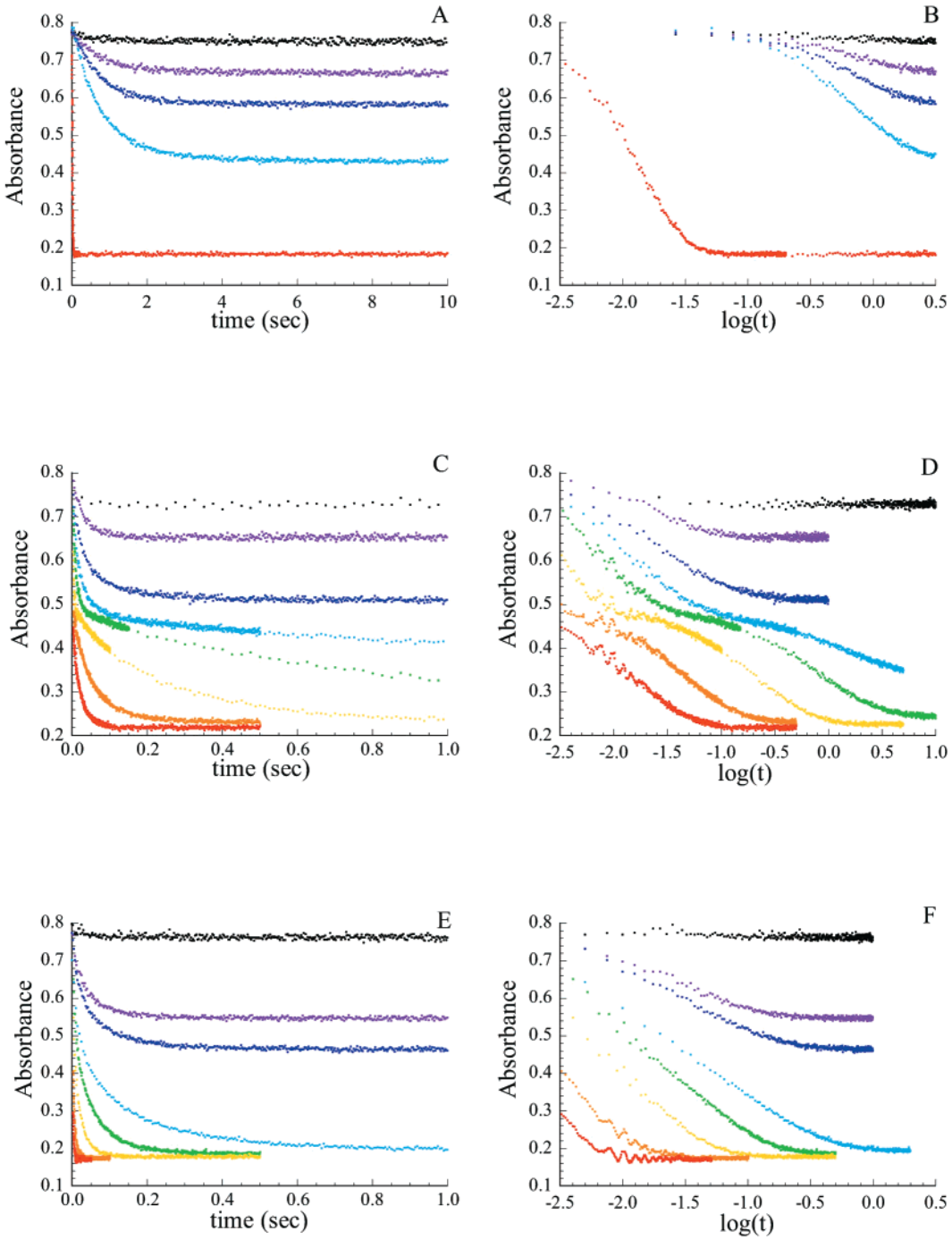

FIGURE 10: Kinetics of CO binding to proximally detached hemoglobins at low CO concentration. Absolute absorbance values at 440 nm are shown for wild-type deoxy-Hb A (panels A, B), deoxy-rHb (αH87G) (panels C, D), and deoxy-rHb (αH87G/βH92G) (panels E and F); concentrations of CO after mixing are, in order in increasing reaction amplitude, 0 μM (black), 2.5 μM (purple), 5 μM (dark blue), 10 μM (light blue), 20 μM (green), 50 μM (yellow), 200 μM (orange), and 500 μM (red). Conditions after mixing: 10 μM hemes, 0.1 M sodium phosphate, 10 mM imd, 2.5 mM sodium dithionite, 20 °C.

under different conditions (*56*−*61*).

Differences in the response of α- versus β-chain proximal linkages to quaternary structure in distally liganded Hbs have also been noted in other studies. The bonds between the proximal histidines and the heme irons in the α-chains (but not the β-chains) break when NO-liganded Hb is driven into the T-state by addition of IHP (*62*). These α-chain (but not β-chain) heme-His bonds are also broken in a crystal structure of wild-type HbCN A that has been locked into the T-quaternary structure by lattice forces (*58*), demonstrating considerable tension at this bond in the T-state of distally liganded Hb. The proximal detachment scheme here differs from these studies in that here the iron-histidine bonds are retained, but the bonds between the histidine side chains and the F-helices are broken. Nonetheless, the studies listed above (*58*, *62*) are consistent with the proximal detachment results here, which indicate that the T-quaternary structure is compatible with the β-, but not the α-chain proximal linkages, when distal ligands are bound. In another study of the relationship between proximal linkages and quaternary structure, Fujii et al. (*63*) prepared Hb derivatives in which either the α-chains or the β-chains contain porphyrins that

Table 4: Kinetic Parameters for Carbon Monoxide Binding at High Concentration to Proximally Detached Hemoglobins[a]

		single exponential	biexponential fitting			
protein	[IHP] mM	k mM^{-1} s^{-1}	k_1 mM^{-1} s^{-1}	%1	k_2 mM^{-1} s^{-1}	%2
wild-type Hb A	0	155 (151, 159)	nd[c]			
wild-type Hb A[b]	1	95	nd[c]			
rHb (αH87G)	0	91.5 (83, 100)	183 (187, 179)	45 (41, 49)	68 (65, 71)	55 (59, 51)
rHb (αH87G)	1	47	90	49	32	51
rHb (βH92G)	0	474 (598, 351)	1090 (1560, 700)	87 (91, 84)	171 (290, 52)	13 (9, 16)
rHb (βH92G)	1	230	852	72	150	28
rHb (αH87G/βH92G)	0	885 (878, 892)	nd[c]			
rHb (αH87G/βH92G)	1	624 (14)	nd[c]			

[a] 500 μM CO after mixing. Although subsequent injections yielded fitted rate constants that differed by less than 10 percent, larger differences were seen when fresh samples and buffers were prepared and reactions were measured on different days. The results of such measurements are presented as the mean value, with values from different days given in parentheses. [b] Determined by C.-K. Hu in the laboratory of C.H. [c] Not determined because progress curves are well-fitted using a single exponential.

lack metal ions (protoporphyrin IX; PP). In these derivatives, where the metal-proximal histidine bonds are permanently missing at half of the heme sites, T-state quaternary structural markers are also retained in ^{1}H NMR spectra when CO is bound to the subunits that retain heme irons. Like the proximal detachment studies here, these T-markers appear to be retained at higher intensity when the iron-histidine bonds are absent from the α-chains [α(PP)$_2$/β(Fe-CO)$_2$, analogous to rHbCO (αH87G) in the present study] than when the bonds are absent from the β-chains [α(Fe-CO)$_2$/β(PP)$_2$, analogous to rHbCO (βH92G)] (*63*). However, in the present study, T-state markers could not be seen under any conditions for rHbCO (βH92G), whereas these markers are clearly present in α(Fe-CO)$_2$/β(PP)$_2$ (*63*). This difference in behavior may be related to a fundamental difference between these two systems. Although the linkage is broken in both systems, in the proximally detached Hbs described here, the iron remains in place in all four hemes and binds distal ligands reversibly to all four subunits. Thus, the absence of T-state markers in the ^{1}H NMR spectrum of rHbCO (βH92G) may result from interactions between the distal ligands and the protein matrix in the β-chains that destabilize the T-state, as well as from proximal restraint in the α-chains. These β-chain distal interactions are absent in the analogous (Fe-CO)$_2$/β(PP)$_2$ since distal ligands cannot bind to the metal-free β-chains.

Table 5: Fitted Parameters for Carbon Monoxide Binding at Low Concentrations to Proximally Detached Hemoglobins

[CO] (μM)[a]	fitted constant[b]	wild-type Hb A	rHb (αH87G)	rHb (βH92G)	rHb (αH87G/βH92G)
2.5	k_{bi}	130	4330	2900	3900
5	k_{bi}	160	9550	2500	4000
10	k_{bi}	190	nd[c]	2200	8600
20	k_{bi}	nd	nd[c]	2000	4700
50	k_{bi}	nd	nd[c]	1600	4100
200	k_{bi}	nd	nd[c]	1200	1600
500	k_{bi}	140	nd[c]	140	300
500	k_{app}	155	100	470	890
50	k_1	nd[c]	4100	nd[c]	nd[c]
50	k_2	nd[c]	80	nd[c]	nd[c]

[a] Total concentration of CO after mixing; total Hb concentration after mixing was 10 μM. [b] All rate constants have units of mM^{-1} s^{-1}. Bimolecular rate constants k_{bi} result from fitting eq 5. For CO concentrations of 10 μM and lower, the starting concentration of CO was adjusted during the fit, and A_{HbCO} was held constant at a value determined independently from a solution of saturated HbCO. For CO concentrations greater than 10 μM, the starting concentration of CO was fixed to its experimentally determined value, and A_{HbCO} was adjusted during the fit. k_{app} is the result of fitting a single exponential (eq 1). k_1 and k_2 result from fitting a biexponential (eq 2). [c] rHb (αH87G) showed clear biexponential behavior above 10 μM CO, so single biexponential fitting (k_{bi}) was not attempted. Since the other Hbs did not show biexponential behavior, only rHb (αH87G) was fitted with two exponentials (k_1 and k_2).

Subunit Dissociation. One route to learning about allostery in Hb A is measurement and comparison of dimer−tetramer assembly free energies of deoxy-, partly, and fully distally liganded Hbs (*9*, *18*). A fundamental result of such studies is that tetramers of deoxy-Hb A are more stable than tetramers of distally liganded Hb A by around 6 kcal/mol (*18*). If the proximal linkages mediate this distal ligand-induced destabilization of the T-quaternary structure, causing tetrameric Hb A to convert to the R-quaternary structure, then removal of the proximal linkages should allow tetrameric Hb A to remain in the T-quaternary structure without destabilization after distal ligands have bound. Thus, proximally detached HbCOs should more stable with respect to subunit dissociation than wild-type Hb A.

Velocity sedimentation experiments on wild-type and proximally detached HbCOs suggest that rHbCO (αH87G) retains significant tetramer stability (Table 2). Combined with the observation by ^{1}H NMR and by near-UV CD that rHbCO (αH87G) retains T-state quaternary structural elements, it appears that, as predicted by Perutz, in that the α-chains proximal linkage destabilizes the HbCO tetramer. The observation that rHbCO (αH87G) and wild-type HbCO are in the same aggregation state has been confirmed using light-scattering experiments to determine translational diffusion coefficients (D. B., E. Bucci, D. Arosio, unpublished).

In contrast to rHbCO (αH87G), velocity sedimentation experiments indicate that the rHbCO (βH92G) tetramer is less stable than the wild-type HbCO tetramer (Table 2). If a spherical shape is assumed for dimeric and tetrameric forms of Hb, molecular weights should scale as the S-values to the three-halves power (*64*). With this approximation, the ratio of the molecular weight of rHbCO (βH92G) to that of rHbCO (αH87G) is calculated to be $(2.81/4.14)^{3/2}$ or 0.56. This crude analysis suggests that whereas rHbCO (αH87G) remains tetrameric, rHbCO (βH92G) is mostly dimeric. Thus, unlike the α-chain proximal linkage, the β-chain proximal linkage appears to stabilize the HbCO tetramer against dissociation: in the absence of the β-chain proximal linkage (βH92G HbCO), the tetramer falls apart. These conclusions are consistent with results from ^{1}H NMR and CD that show that T-state quaternary structure markers are lost in rHbCO

(*β*H92G); rather than conversion to the R-quaternary structure as is seen for wild-type HbCO, these markers appear to be lost to dissociation. The mechanism by which the *β*-chain proximal linkage stabilizes the HbCO tetramer is not obvious to us.

For the fully proximally detached rHbCO (αH87G/*β*H92G), velocity sedimentation experiments also show a decreased sedimentation coefficient as compared to wild-type HbCO and rHbCO (αH87G), although the decrease is more modest than that seen for rHbCO (*β*H92G) (Table 2). Assuming spherical shape, the ratio of the S-value of rHbCO (αH87G/*β*H92G) to rHbCO (αH87G) indicates a molecular weight ratio of $(3.51/4.14)^{3/2}$ or 0.78, suggesting a mix of dimers and tetramers for rHbCO (αH87G/*β*H92G). Thus, it appears that the tetramer dissociation that is produced by proximal detachment in the *β*-chains is partly compensated for by α-chain proximal detachment, consistent with the idea that the α-chain proximal linkages destabilize the HbCO tetramer, and its deletion stabilizes the tetramer. These results are supported by ^{1}H NMR and CD studies, where α-chain proximal detachment in the *β*-detached background restores T-state markers, albeit to a limited degree.

Relative Equilibrium Affinities of the α- *and β-Chains of rHb (*α*H87G).* Titration of the ^{1}H NMR spectrum of deoxy-rHb (αH87G) with *n*-buNC clearly shows binding site heterogeneity to play a large role in the stretched equilibrium binding curve measured for this mutant using absorbance spectroscopy (*17*). On the basis of the assignments made using deuterated imd, the α-chains of this proximally detached protein have higher affinity for distal ligand than the *β*-chains. Since the α-chain is detached in this mutant, these observations indicate that proximal detachment increases distal ligand affinity in the T-state, confirming that in the T-state, proximal restraint limits reactivity. In the *β*-chains of rHb (αH87G), where the proximal linkages remain intact, proximal restraint decreases affinity.

A quantitative estimate of the contribution of proximal restraint in limiting T-state reactivity can be obtained by comparing midpoints for the two phases in the binding curves. Fitting absorbance *n*-buNC titration data with a two-site noninteracting model yields binding constants that differ by around 6-fold (*17*). These values can be compared with binding constants determined by Reisberg and Olson (*65*) for *n*-buNC to the α- and *β*-chains of the T- and R-states of wild-type Hb A (Figure 11, panel A). Although the proximally detached α-chain has enhanced affinity (a lower midpoint) for *n*-buNC as compared with the *β*-chain, its affinity is not as large as the α-chain of the R-state of wild-type Hb A. Similarly, the *β*-chain of rHb (αH87G) has low affinity for *n*-buNC, but it is not as low as the *β*-chain of the T-state of wild-type Hb A. Thus, it appears that for *n*-buNC, reactivity at the α-chains is also limited by nonproximal interactions, such as those between bound *n*-buNC and side chains in the distal pocket.

Kinetics of Distal Ligand Binding and Dissociation from Wild-Type Hb A. The progressive enhancement of distal ligand affinity as the number of bound distal ligands increases has its origins in both a progressive increase of the rate of ligand binding and a progressive decrease in the rate of ligand dissociation, as distal ligand occupancy increases (*2*, *66*−*70*). These changes in the rate of distal ligand binding and dissociation have been represented using a kinetic Adair-

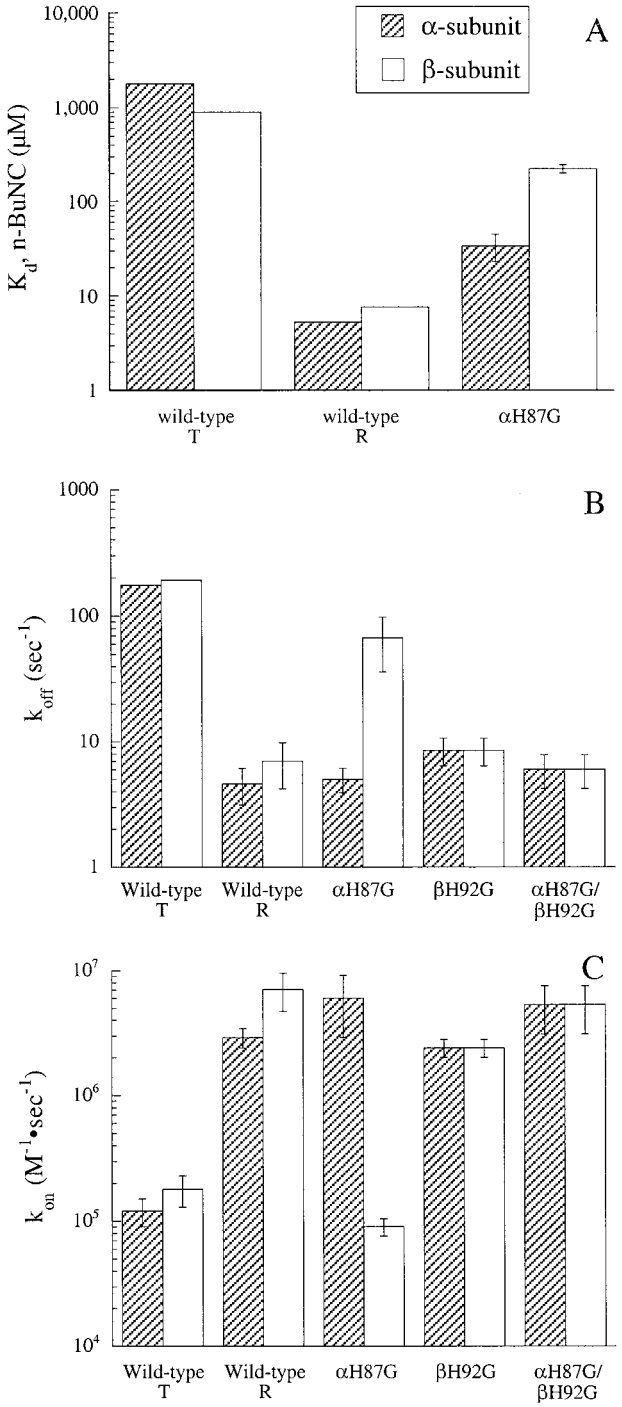

FIGURE 11: Comparison of distal ligand rate and equilibrium constants for proximally detached Hbs with T- and R-state hemoglobin. *n*-buNC equilibrium constants (A), CO off-rates (B), and CO on-rates (C) for α- and *β*-chains (stippled and open bars, respectively). For rHb (*β*H92G) and rHb (αH87G/*β*H92G), kinetic phases were not resolved, so the same values are reported for both chains. Association rate constants for proximally detached Hbs are from fits at low CO concentration for the fast phase of rHb (αH87G) and for the entire progress curves of rHbs (*β*H92G) and (αH87G/*β*H92G), and from fits at high CO concentration for the slow phase of rHb (αH87G) (Table 5). Equilibrium constants for *n*-buNC binding to wild-type Hb A are from Reisberg and Olson (*65*). Association rate constants for T- and R-state Hb, dissociation rate constants for R-state HbCO, and uncertainty estimates are taken from ref *12*. Values for CO dissociation rate constants from the T-state of Hb A are from studies of nickel and magnesium-substituted Hbs (*74*). Similar values are obtained for T-state HbCO dissociation rate constants through the relation $k_{off}^T = 13k_{off}^R$ from ref *68*, using values of k_{off}^R from ref *12*.

type scheme containing eight stepwise rate constants, and as a simpler kinetic Monod−Wyman−Changeux (MWC) model in which rate constants are determined by just two quaternary structures (T and R) (*12*, *68*). The latter treatment has fewer variables and has recently gained support from sophisticated kinetic analyses that span 7 orders of magnitude of time (*71*), although recent kinetic measurements of ligand binding in metal substituted Hbs suggest that more than two states are necessary to explain ligand reactivity in Hb A (*72*). Here, we base our discussion of the kinetics of CO binding and dissociation on the simpler kinetic MWC model (*12*, *68*).[3] The time course of association of CO to wild-type deoxy-Hb A should be dominated by distal ligand binding to the T quaternary structure, with a second-order rate constant close to that of the T-state association constant (*73*). Because subsequent association reactions are of an equal or faster rate, they increase the amplitude of the progress curve but are otherwise invisible behind the slow, rate-limiting step of binding the first ligand. The time course for dissociation of CO from wild-type HbCO should be dominated by distal ligand dissociation from the R-quaternary structure and should be first order. Because NO binds very fast in the kinetic competition experiments, dissociation rarely proceeds past one free heme site; thus, the observed dissociation time course results from the conversion from $Hb(CO)_4$ to $Hb(CO)_3$.

Anticipated Kinetic Effects of Proximal Detachment. We have shown previously (*17*) that detachment of the proximal histidines increases distal ligand affinity and decreases cooperativity. If T-state structure persists after distal ligand binding [as it does for rHbCO (αH87G) and, to a lesser extent, for rHbCO (αH87G/*β*H92G)], the increase in distal ligand affinity in proximally detached Hbs indicates that part of the enhancement in affinity in the R-state of wild-type Hb A results from relief of proximal restraint, as predicted by the Perutz mechanism. However, whether relief of proximal restraint accounts for the entire affinity difference between T- and R-state Hb cannot be determined without making quantitative measurements of distal ligand reactivity that isolate the T- and R-states. As described above, kinetic studies provide an effective means to isolate the T- and R-state reactivities. By examining the kinetics of distal ligand binding and release from our proximally detached Hbs, we should be able to determine the relative roles of proximal restraint relief versus distal mechanisms in modulating distal ligand affinity between T- and R-state Hb, and will determine which side of the ligand barrier proximal and distal effects are partitioned on.

If the polypeptide surrounding the distal ligand binding sites plays no direct role in modulating distal ligand affinity between T versus R, proximal detachment should affect rates of distal ligand association but not dissociation. In this all-proximal limit, the time course of distal ligand association should be accelerated by proximal detachment, because detachment frees the heme irons from the low-affinity proximal restraints of the polypeptide in its T quaternary structure. Conversely, the time course of distal ligand dissociation rates in this all-proximal limit should be insensitive to proximal detachment in comparison to wild-type HbCO A, dissociating at the R-state rate despite a T-state distal pocket.

If the polypeptide surrounding the distal ligand binding sites also plays a role in modulating distal ligand affinity between T versus R states, proximal detachment should affect both the rates of distal ligand association and dissociation. Rates of distal ligand association to proximally detached Hbs should be enhanced relative to wild-type deoxy-Hb A because proximal restraint is released by detachment, but because the T-quaternary structure persists in the proximally detached Hbs, binding may not be as fast as to the R-state of wild-type Hb A. Rates of distal ligand dissociation should be increased, because the proximally detached Hbs remain in the T-state, destabilizing distal ligand and promoting fast release. Of course, the degree to which both proximal and distal interactions affect rates will also depend on which side of the kinetic barrier these interactions occur.

Kinetic Effects of Detachment in rHb (αH87G). Since rHb (αH87G) remains a tetramer in the distal ligand-saturated form, and since ^{1}H NMR and CD indicate that rHb (αH87G) remains in the T-state with distal ligand bound, the results of kinetic and equilibrium studies provide an assessment of the contribution of proximal restraint to the low distal ligand reactivity of the T-state of Hb. The proximally detached α-chains remain in the T-state but are free from proximal restraint, whereas the *β*-chains are stuck in the T-state and remain under proximal restraint. However, to determine the effects of proximal restraint in the T-state, it is necessary to assign the relevant portions of kinetic progress curves to the α- and *β*-chains. In the case of the equilibrium *n*-BuNC binding curve for rHb (αH87G), this assignment was made using ^{1}H NMR (Figure 6), which showed the α-chains to be high in affinity as compared to the *β*-chains. Although equilibrium binding curves for CO have not been measured because of very high affinities, O_2 binding to rHb (αH87G) also shows biphasic behavior (*17*). Assuming that CO also binds with such biphasic characteristics, and that the two phases are the result of high affinity α-chains and low affinity *β*-chains, it seems reasonable to assign the fast phase of CO binding to the high affinity α-chains, and the fast phase in CO dissociation to the low affinity *β*-chains. However, definitive assignments will require second-site modification, as was done by Matthews and Olson (*12*).

Assuming the slow kinetic phase in CO dissociation is from the α-chain, CO dissociates from the proximally detached α-chains of rHbCO (αH87G) at nearly the same rate as from the α-chains of wild-type HbCO A in the R-state, although the protein retains the T-quaternary structure (Figure 11, panel B). Thus, dissociation rates in the α-subunits are controlled by the proximal linkage, rather than by the tertiary and quaternary structure of the surrounding T-state protein matrix. CO dissociation from the *β*-chains of rHbCO (αH87G) occurs at a rate close to that of the *β*-chains of wild-type HbCO in the T-state (the measured rate constant is three times smaller than that of the wild-type *β*-chain T-state, and 10 times larger than that for the wild-type R-state [Figure 11, panel B]). Given that the *β*-chains of rHbCO (αH87G) are in the T-quaternary structure and are subject to proximal restraint, it is not

[3] The extensions of the MWC model by Henry et al. to include stretched exponentials and geminate recombination (*71*) are not required in our studies, because on the slow time-scale of the reactions that we monitor, thermal averaging of conformational substates should be complete.

unexpected that the rate of CO dissociation from the β-chains should approach the wild-type HbCO A T-state rate. Although modest, the 3-fold decrease in CO dissociation rate from the β-chains of rHb (αH87G) as compared to the wild-type T-state rate may be an indication that there are some allosteric effects still operative at the β-chains that enhance reactivity despite the presence of T-quaternary structure and proximal restraint. Such allostery may result either from interactions between β-chains or from interactions transmitted to the β-chains from the distal faces of the α-chains. Residual allostery in distal ligand binding to the β-chain of rHb (αH87G) is also suggested in the comparison of equilibrium affinities of rHb (αH87G) for *n*-buNC to affinities of *n*-buNC for the T- and R-states of wild-type Hb A (Figure 11, panel A). The β-chains of rHb (αH87G) are around four times more reactive than the β-chains in the T-state of wild-type Hb A (Figure 11, panel A).

Comparison of the rate constants for CO association with rHb (αH87G) to those of wild-type Hb A shows that CO binds to the β-chains of rHb (αH87G) at rates close to those seen for the T-state of wild-type Hb A. Again, since the β-chains are still proximally restrained, and since the rHb (αH87G) remains in the T-state, low reactivity is expected at the β-chains. The residual allostery that may be seen in CO dissociation is not detected in CO association (Figure 11, panel C). Thus, residual allostery of distal ligand binding to rHb (αH87G) may be kinetically partitioned exclusively into dissociation rates, although kinetic cooperativity in association may go undetected, because the kinetic enhancement would follow the slow step in distal ligand binding. In contrast with the β-chains of rHb (αH87G), the α-chains bind CO at a rate comparable to the R-state of wild-type Hb A. Thus, as with CO dissociation, CO binding to the α-chains appears to be controlled entirely by proximal restraint. This picture differs somewhat from the distal ligand *n*-buNC, where reactivity of the α-chains of rHb (αH87G) is lower than that of the α-chains of R-state wild-type Hb A (Figure 11, panel A). Thus, the allosteric properties of different distal ligands may result from different interactions with the protein matrix. Larger ligands such as *n*-buNC may be more sensitive to distal interactions.

The kinetic studies presented here show the effects of proximal restraint to be partitioned into both distal ligand binding and dissociation. The rate of CO binding to the α-chains of rHb (αH87G) is increased as compared to wild-type T-state Hb, and the rate of CO dissociation from the α-chains of rHbCO (αH87G) is decreased as compared to wild-type T-state HbCO. This observation indicates that in the T-state, proximal restraint partially destabilizes the transition state for binding, but the degree of destabilization is less than for fully bound CO. These results are consistent with heme studies, which show that proximal restraint inhibits CO binding and speeds CO dissociation (*28*).

Kinetic Effects of Detachment in rHb (βH92G) and in rHb (αH87G/βH92G). Because significant dissociation to dimers is seen for rHbCO (βH92G), kinetic profiles are not as readily interpretable as for the tetrameric rHb (αH87G). Unlike the kinetic curves seen for rHb (αH87G), there is no evidence of kinetic heterogeneity for rHb (βH92G) (Figures 7 and 9). Since in wild-type Hb A, $\alpha\beta$ dimers react as if in the R-state (*39*), it is likely that the high degree of tetramer dissociation in the CO form of rHb (βH92G) eliminates the off-rate enhancement of the T-quaternary structure, producing slow dissociation rates for α- as well as β-chains (Table 3, Figure 11, panel B). In contrast, it appears from rates of CO binding to rHb (βH92G) that there may be some T-state restraint limiting distal ligand binding: although CO binds faster than to wild-type T-state Hb, binding is slightly slower than to wild-type R-state Hb, especially at the β-chain (Figure 11, panel C). That the T-state is acting to decrease the rate of distal ligand binding in rHb (βH92G) is also supported by the observation that IHP, which acts on the T-state, significantly slows the rate of distal ligand binding.

For rHbCO (αH87G/βH92G), where tetramer dissociation is reduced, and where partial T-state quaternary structure persists in the CO form, slow distal ligand dissociation rates are expected from both α- and β-chains, because proximal restraint is relieved in all subunits. Indeed, the fitted rate constant for CO dissociation from rHbCO (αH87G/βH92G) (0.006 s^{-1}) is midway between the values seen for the α- and β-chains of the R-state of wild-type Hb A (0.0046 and 0.0072 s^{-1}, respectively). Of course, the data are also consistent with slow dissociation from $\alpha\beta$ dimers. The apparent distal ligand association rate constant in rHb (αH87G/βH92G) is roughly equal to that of the R-state of wild-type Hb A; again this may either be a result of loss of proximal restraint or of partial loss of tetrameric structure.

SUMMARY

The results here are consistent with the Perutz model for cooperative distal ligand binding in Hb. Elimination of proximal restraint increases reactivity in the T-state, as seen for the α-subunits of rHb (αH87G). For CO, kinetic studies suggest that this enhancement is as great as for the R-state of wild-type Hb A, despite the persistence of the T-state structure. For *n*-buNC, it appears that some residual allostery may still be operative. Although the tendency of rHbCO (βH92G) to dissociate prevents a similar analysis of proximal restraint in the β-subunits, quaternary structure studies demonstrate that the proximal linkages of the α- and β-chains have different effects on the T-state of distally liganded Hb.

ACKNOWLEDGMENT

We thank Dr. John S. Olson for critical reading of an early version of this manuscript and for suggesting that a fast phase of CO binding would be revealed at low CO concentration. We thank Dr. Walt Baase for help with circular dichroism spectroscopy. We thank Dr. Richard DeSa and Dr. Ching-Hsuan Tsai for advice and assistance with stopped-flow measurements, and Dr. Rick Dahlquist for critical discussion. D.B. acknowledges the Helen Hay Whitney Foundation, the Arnold and Maybel Beckman Foundation, and the Oregon Affiliate of the American Heart Association for financial support.

REFERENCES

1. Wyman, J. (1964) *Adv. Protein Chem. 19*, 223−268.
2. Antonini, E., and Brunori, M. (1971) *Hemoglobin and Myoglobin in Their Reaction with Ligands*, North-Holland Publishing Company, London.
3. Imai, K. (1982) *Allosteric Effects in Haemoglobin*, Cambridge University Press, Cambridge.

4. Wyman, J., and Gill, S. J. (1990) *Binding and Linkage. Functional Chemistry of Biological Macromolecules*, University Science Books, Mill Valley.
5. Perutz, M. F. (1970) *Nature 228*, 726−39.
6. Baldwin, J., and Chothia, C. (1979) *J. Mol. Biol. 129*, 175−220.
7. Nagai, K., Luisi, B., Shih, D., Miyazaki, G., Imai, K., Poyart, C., De Young, A., Kwiatkowsky, L., Noble, R. W., Lin, S. H., and et al. (1987) *Nature 329*, 858−60.
8. Olson, J. S., Mathews, A. J., Rohlfs, R. J., Springer, B. A., Egeberg, K. D., Sligar, S. G., Tame, J., Renaud, J. P., and Nagai, K. (1988) *Nature 336*, 265−6.
9. Ackers, G. K., Doyle, M. L., Myers, D., and Daugherty, M. A. (1992) *Science 255*, 54−63.
10. Englander, S. W., Englander, J. J., McKinnie, R. E., Ackers, G. K., Turner, G. J., Westrick, J. A., and Gill, S. J. (1992) *Science 256*, 1684−7.
11. Kim, H. W., Shen, T. J., Sun, D. P., Ho, N. T., Madrid, M., Tam, M. F., Zou, M., Cottam, P. F., and Ho, C. (1994) *Proc. Natl. Acad. Sci. U.S.A. 91*, 11547−51.
12. Mathews, A. J., and Olson, J. S. (1994) *Methods Enzymol. 232*, 363−86.
13. Rodgers, K. R., and Spiro, T. G. (1994) *Science 265*, 1697−9.
14. Jayaraman, V., Rodgers, K. R., Mukerji, I., and Spiro, T. G. (1995) *Science 269*, 1843−8.
15. Olson, J. S., and Phillips, G. N., Jr. (1996) *J. Biol. Chem. 271*, 17593−6.
16. Huang, S., Peterson, E. S., Ho, C., and Friedman, J. M. (1997) *Biochemistry 36*, 6197−206.
17. Barrick, D., Ho, N. T., Simplaceanu, V., Dahlquist, F. W., and Ho, C. (1997) *Nat. Struct. Biol. 4*, 78−83.
18. Ackers, G. K. (1998) *Adv. Protein Chem. 51*, 185−253.
19. Ho, C., Sun, D. P., Shen, T. J., Ho, N. T., Zou, M., Hu, C. K., Sun, Z. Y., and Lukin, J. A. (1998) in *Blood Substitutes-Present and Future Perspectives* (Tsuchida, E., Ed.) pp 281−296, Elsevier Science S. A., Lausanne.
20. Ho, C., and Lukin, J. A. (2000) in "Hemoglobin: Cooperativity in Protein-Ligand Interactions" in *Embryonic Encyclopedia of Life Sciences*. MacMillan References, Ltd., London. www.els.net.
21. Tsai, C. H., Shen, T. J., Ho, N. T., and Ho, C. (1999) *Biochemistry 38*, 8751−61.
22. Inaba, K., Ishimori, K., Imai, K., and Morishima, I. (2000) *J. Biol. Chem. 275*, 12438−45.
23. Warshel, A. (1977) *Proc. Natl. Acad. Sci. U.S.A. 74*, 1789−93.
24. Gelin, B. R., and Karplus, M. (1977) *Proc. Natl. Acad. Sci. U.S.A. 74*, 801−5.
25. Perutz, M. F. (1990) *Mechanisms of Cooperativity and Allosteric Regulation in Proteins*, Cambridge University Press, Cambridge.
26. Collman, J. P., and Reed, C. A. (1973) *J. Am. Chem. Soc. 95*, 2048−9.
27. Brault, D., and Rougee, M. (1974) *Biochem. Biophys. Res. Commun. 57*, 654−9.
28. White, D. K., Cannon, J. B., and Traylor, T. G. (1979) *J. Am. Chem. Soc. 101*, 2443−2454.
29. Collman, J. P., Brauman, J. I., Doxsee, K. M., Halbert, T. R., and Suslick, K. S. (1978) *Proc. Natl. Acad. Sci. U.S.A. 75*, 564−8.
30. Shen, T. J., Ho, N. T., Simplaceanu, V., Zou, M., Green, B. N., Tam, M. F., and Ho, C. (1993) *Proc. Natl. Acad. Sci. U.S.A. 90*, 8108−12.
31. Philo, J. S. (1994) in *Modern Analytical Ultracentrifugation*, pp 156−170, Birkhauser Publishing Co, Boston.
32. Philo, J. S. (1997) *Biophys. J. 72*, 435−44.
33. Plateau, P., and Gueron, M. (1982) *J. Am. Chem. Soc. 104*, 7310−7311.
34. Gray, R. D., and Gibson, Q. H. (1971) *J. Biol. Chem. 246*, 7168−74.
35. Olson, J. S. (1981) *Methods Enzymol. 76*, 631−51.
36. Simon, S. R., and Cantor, C. R. (1969) *Proc. Natl. Acad. Sci. U.S.A. 63*, 205−12.
37. Perutz, M. F., Ladner, J. E., Simon, S. R., and Ho, C. (1974) *Biochemistry 13*, 2163−73.
38. Woody, R. (1978) in *Biochemical and Clinical Aspects of Hemoglobin Abnormalities* (S, C. W., Ed.), Academic Press, New York.
39. Mills, F. C., Johnson, M. L., and Ackers, G. K. (1976) *Biochemistry 15*, 5350−62.
40. Svedberg, T., and Nichols, J. (1927) *J. Am. Chem. Soc. 49*, 2920.
41. Field, E. O., and O'Brien, J. R. P. (1955) *Biochem. J. 60*, 656.
42. Rossi-Fanelli, A., Antonini, E., and Caputo, A. (1964) *Adv. Protein Chem. 19*, 73−777.
43. Russu, I. M., Ho, N. T., and Ho, C. (1987) *Biochim. Biophys. Acta 914*, 40−8.
44. Craescu, C. T., and Mispelter, J. (1989) *Eur. J. Biochem. 181*, 87−96.
45. Fung, L. W., and Ho, C. (1975) *Biochemistry 14*, 2526−35.
46. Ho, C. (1992) *Adv. Protein Chem. 43*, 153−312.
47. Simplaceanu, V., Lukin, J. A., Fang, T. Y., Zou, M., Ho, N. T., and Ho, C. (2000) *Biophys. J. 79*, 1146−54.
48. Arnone, A., and Perutz, M. F. (1974) *Nature 249*, 34−6.
49. Takahashi, S., Lin, A. K., and Ho, C. (1980) *Biochemistry 19*, 5196−202.
50. La Mar, G. N., Budd, D. L., and Goff, H. (1977) *Biochem. Biophys. Res. Commun. 77*, 104−10.
51. La Mar, G. N., Dalichow, F., Zhao, X., Dou, Y., Ikeda-Saito, M., Chiu, M. L., and Sligar, S. G. (1994) *J. Biol. Chem. 269*, 29629−35.
52. Takahashi, S., Lin, A. K., and Ho, C. (1982) *Biophys. J. 39*, 33−40.
53. Fetler, B. K., Simplaceanu, V., and Ho, C. (1995) *Biophys. J. 68*, 681−93.
54. Barrick, D. (2000) *Proteins 39*, 291−308.
55. Reisberg, P. I., and Olson, J. S. (1980) *J. Biol. Chem. 255*, 4144−30.
56. Silva, M. M., Rogers, P. H., and Arnone, A. (1992) *J. Biol. Chem. 267*, 17248−56.
57. Smith, F. R., Lattman, E. E., and Carter, C. W., Jr. (1991) *Proteins 10*, 81−91.
58. Paoli, M., Dodson, G., Liddington, R. C., and Wilkinson, A. J. (1997) *J. Mol. Biol. 271*, 161−7.
59. Srinivasan, R., and Rose, G. D. (1994) *Proc. Natl. Acad. Sci. U.S.A. 91*, 11113−7.
60. Liddington, R. (1994) *Methods Enzymol. 232*, 15−26.
61. Mueser, T. C., Rogers, P. H., and Arnone, A. (2000) *Biochemistry 39*, 15353−15364.
62. Perutz, M. F., Kilmartin, J. V., Nagai, K., Szabo, A., and Simon, S. R. (1976) *Biochemistry 15*, 378−87.
63. Fujii, M., Hori, H., Miyazaki, G., Morimoto, H., and Yonetani, T. (1993) *J. Biol. Chem. 268*, 15386-93.
64. Cantor, C. R., and Schimmel, P. R. (1980) *Biophysical Chemistry: Techniques for the Study of Biological Structure and Function*, Vol. 2, W. H. Freeman & Company, New York.
65. Reisberg, P. I., and Olson, J. S. (1980) *J. Biol. Chem. 255*, 4159−69.
66. Roughton, F. J. W., Otis, A. G. B., and Lyster, R. L. J. (1955) *Proc. Royal Soc. B 144*, 29−54.
67. Gibson, Q. H. (1959) *Prog. Biophys. Chem. 9*, 1−53.
68. Hopfield, J. J., Shulman, R. G., and Ogawa, S. (1971) *J. Mol. Biol. 61*, 425−43.
69. MacQuarrie, R., and Gibson, Q. H. (1972) *J. Biol. Chem. 247*, 5686−94.
70. Sawicki, C. A., and Gibson, Q. H. (1978) *Biophys. J. 24*, 21−33.
71. Henry, E. R., Jones, C. M., Hofrichter, J., and Eaton, W. A. (1997) *Biochemistry 36*, 6511−28.
72. Gibson, Q. H. (1999) *Biochemistry 38*, 5191−9.
73. Mathews, A. J., Olson, J. S., Renaud, J. P., Tame, J., and Nagai, K. (1991) *J. Biol. Chem. 266*, 21631−9.
74. Unzai, S., Eich, R., Shibayama, N., Olson, J. S., and Morimoto, H. (1998) *J. Biol. Chem. 273*, 23150−9.

BI002165Q